Research article

Journal of RAMAN SPECTROSCOPY

Received: 3 August 2012 Revised: 10 January 2013 Accepted: 11 January 2013 Published online in Wiley Online Library: 1 March 2013

(wileyonlinelibrary.com) DOI 10.1002/jrs.4277

A first principles lattice dynamics and Raman spectra of the ferroelastic rutile to $CaCl_2$ phase transition in SnO_2 at high pressure

Sanjay D. Gupta,[a] Sanjeev K. Gupta,[a] Prafulla K. Jha[a]* and N. N. Ovsyuk[b]

A first principles calculation of the lattice dynamical properties of rutile SnO_2 has been performed using density functional perturbation theory at ambient and high-pressure conditions to understand the pressure-induced phase transition. The calculated zone centre phonon modes at ambient and high pressures have been compared with Raman scattering and infrared measurements. Full phonon dispersion curves and phonon densities of states and Raman intensities at high pressures are calculated and given for the first time in literature. The ferroelastic transition from the rutile to the $CaCl_2$-type structure was confirmed. It is clearly illustrated that the first transition is associated with macroscopic shear instability which arises from the strong coupling between elastic constants and softening of Raman active B_{1g} mode. The observed pressure of phase transition in experimental measurements was reproduced more accurately than in previous calculations, and the difference between observed and calculated transition pressure is only of the order of 2%. The mode Grüneisen parameter is quantitatively as well as qualitatively different from the earlier reported values. Copyright © 2013 John Wiley & Sons, Ltd.

Keywords: Density functional theory; Phonons in crystal lattices; High-pressure effects; Ferroelastic, SnO2; High Pressure Raman spectra

Introduction

Tin oxide (SnO_2) is one of the most important materials from the group of transparent conducting oxides and received a great deal of interest for many years due to several fields of application such as solar cells, optoelectronic devices, touch screen, oxidation catalysts, light emitting diodes etc..[1–3] Under ambient conditions, SnO_2 crystallizes in a rutile-type structure with $P4_2/mnm$ (D_{4h}^{14}) symmetry with six atoms per unit cell[4,5] and therefore is isostructural to many other AO_2 compounds including stishovite (rutile-type structure) which is the high-pressure polymorph of silica.[6–12] Investigations have predicted that the SnO_2 exhibits two following sequence of high-pressure phase transition from rutile to $CaCl_2$ type to the α-PbO_2 type and finally to the pyrite type.[13–23] The most common phase transition under pressure is the $CaCl_2$-type structure which is closely related to the rutile structure. The symmetry of the $CaCl_2$-type structure is orthorhombic with space group Pnnm, a direct subgroup of $P4_2/mnm$.[18] This direct group–subgroup relationship indicates a possible second-order ferroelastic phase transition driven by the B_{1g} phonon mode.[18] Modern ab initio density functional theory (DFT) offers these days a parameter free calculation of phase transition even in complex systems. However, the standard method for the calculation of relative stability of high-pressure phase usually based on the examination of pressure-dependent energy for different phases leads to uncertainty to find the stable structures out of all studied crystal structures. The stability of crystal structure is determined by three stability conditions which must be followed simultaneously for a given crystal: (1) Total force on each atom is zero,[24] (2) Crystal lattice is stable against macroscopic displacements such as compression or shear and (3) Crystal lattice is stable against any small displacements, meaning all phonon frequencies are real.[25] It is well known from the soft mode theory[26] of phase transition that the frequency of certain phonon mode approaches zero under the influence of extreme parameters such as temperature, pressure, magnetic field etc.

The motivation of the present study is to investigate the phase transition between rutile and $CaCl_2$ phase of SnO_2 and a large discrepancy between observed 11.8 GPa from x-ray diffraction,[4] 14.2 GPa from Raman spectroscopy[18] and 14.6 GPa from Brillouin spectroscopy[18] and calculated 7 GPa[19] transition pressure values for high-pressure phase transition. It is important to bring in notice that the experimental phase transition pressure in this group of compounds varies due to the several experimental constraints and nature of phase transition.[27] Since the structural change from the rutile phase to the $CaCl_2$ phase is a second-order transition accompanied by a zero or a very small volume change, the determination of the precise transition pressure is a difficult task due to difficulty in identifying the characteristic features of transition pressure: onset of the splitting of associated axes from x-ray study and Raman modes from Raman spectroscopy.[27] Therefore, the quality of x-ray diffraction, Raman or Brillouin spectroscopy influences the uncertainty of the determination of transition pressure. In addition, the degree of stress condition in the sample, i.e. the pressure difference between the centre and the edge of the sample chamber and nonhydrostatic conditions, influences the uncertainty of the

* *Correspondence to: Prafulla K. Jha, Department of Physics, Maharaja Krishnakumasinhji Bhavnagar University, Bhavnagar, India. E-mail: prafullaj@yahoo.com*

a *Department of Physics, Maharaja Krishnakumarsinhji Bhavnagar University, Bhavnagar 364001, India*

b *Institute of Geology and Mineralogy, Siberian Branch, Russian Academy of Sciences, Novosibirsk 630090, Russia*

phase transition pressure.[27] Therefore, a complementary ab initio DFT calculation is quite meaningful.

In SnO_2, the phonon dispersion curves (PDC) are very important, and it is of interest to study the effects of pressure on its lattice dynamical properties. The Raman spectroscopy has been used quite successfully to identify the phase transition.[18,28] There have been few lattice dynamical studies in to the rutile to $CaCl_2$ transition in SnO_2 using both model[29] and ab initio calculations[19] to understand the PDC and find responsible mode which derive the phase transition. Though the study of Parlinski *et al.*[19] was successful in finding the responsible B_{1g} mode to get softened, the predicted transition pressure was quite far from the experiments. Furthermore, despite the importance of Raman spectroscopy in identifying the phase transition, no calculation is so far reported on the pressure-dependent Raman intensity.

In this study, we present systematic theoretical results from ab initio calculations on rutile SnO_2 at pressure up to 20 GPa. The main objective of this work is to determine phase transition pressure between the rutile and $CaCl_2$-type structures and elucidate the inconsistency in transition pressures between observed and predicted. In addition, the SnO_2 is regarded to be a good analogy material for silica (SiO_2), an important component of the Earth's mantle as both SnO_2 and SiO_2 are IV-B metal dioxides. It has been observed that free silica could exist in the subducted oceanic crust in the lower mantle of the earth. However, it lacks an adequate understanding of high-pressure behavior. Studies predict that silica exhibits the sequence of structural phase transitions stishovite (rutile type) to $CaCl_2$ type to α-PbO_2 type to pyrite type. SnO_2 which is analogous to silica shows a similar sequence of phase transitions, although phase boundary has not been determined. The high-pressure phase transition from rutile to $CaCl_2$-type structure is well known in group 14 (SiO_2, GeO_2 and SnO_2) dioxide. Therefore, in order to investigate this phase transition, the low-pressure analog studies are more accessible, particularly using experiments. In that sense, this study reports an important prediction about Raman spectra of SnO_2 for experimentalist. An understanding of SnO_2 analogous to silica would hence make a valuable contribution to the understanding of the transition to the silica polymorphs. In addition the importance of physics and chemical properties of SnO_2 ranges from solid-state gas sensors to transparent conductors to heterogeneous catalysis, and hence there is an obvious close relationship between these properties of SnO_2 and its structures. Better knowledge of high-pressure phases of SnO_2 will be useful to understand the behavior of silica at deep mantle conditions.

Computational details

Calculations were performed using the pseudopotential approximation within the self-consistent plane wave basis sets, implementation of DFT in Quantum Espresso Code[30] with generalized gradient (GGA) and local density approximations (LDA) to exchange correlation energy parameterized by Purdue, Burke and Ernzerhof[31] within norm conserving and ultrasoft pseudopotentials. Both sets of pseudopotential used to perform the computations are based on the electron scalar non-relativistic computations and ultrasoft pseudopotential built using the Vanderbilt ultrasoft schemes[32] in the configuration $5s^2\ 5p^2\ 4d^{10}\ r_c = 1.7$a.u. for Sn and $2s^2\ 2p^4\ r_c = 1.2$a.u for O and $5s^2\ 5p^2\ 4d^{10}$ for Sn and $2s^2\ 2p^4$ for O in the case of ultrasoft and norm-conserving pseudopotentials, respectively. The electronic wave functions are represented in a plane wave basis set with a kinetic energy cutoff of 60 Ry. The Brillouin zone (BZ) integrations are carried out by the Methfessel smearing technique using 6×6×9 k-point mesh with shift from origin. The total energies converged to within 10^{-4} Ry/atom with respect to cutoff energy and k-point mesh. Lattice dynamical calculations (PDC and phonon density of states) are performed within the framework of self-consistent density functional perturbation theory (DFPT).[33] The advantage of DFPT linear response method is that it allows calculating the phonons of any wave vector only using the unit cell.[33] This method has also been quite successfully used to calculate the PDC and provide reliable phase boundaries of high-pressure polymorphs of silica.[34] The dynamical matrices were calculated on a 2×2×3 grid (q-point) sampling, where all the structural parameters are fully relaxed. The calculation of Raman intensities has been obtained, based on Placzek's polarizability theory.[35] The calculated non-resonant Raman intensity associated with the vibrational normal mode Q_i is defined by the following two quantities: (1) the scattering activity coefficient (S_i) and (2) the depolarization ratio (ρ_i) and can be expressed as,

$$S_i = g_i\left[45\left(\alpha_i^{'}\right)^2 + 7\left(\gamma_i^{'}\right)^2\right] \quad (\text{Å}^4/amu), \tag{1}$$

$$\rho_i = \frac{3\left(\gamma_i^{'}\right)^2}{45\left(\alpha_i^{'}\right)^2 + 4\left(\gamma_i^{'}\right)^2} \tag{2}$$

Where, g_i is the degeneracy of the normal mode; $\alpha_i^{'}$ and $\gamma_i^{'}$ are the derivatives of the trace and the anisotropy of the polarizability tensor, respectively.

$$\left(\alpha_i^{'}\right)^2 = \frac{1}{9}\sum_u \left(\frac{\partial \alpha_{uw}}{\partial Q_i}\right)^2, u = x, y, z, \tag{3}$$

$$\left(\gamma_i^{'}\right)^2 = \frac{1}{2}\sum_{uw}\left[3\left(\frac{\partial \alpha_{uw}}{\partial Q_i}\right)^2 - \left(\frac{\partial \alpha_{uu}}{\partial Q_i}\frac{\partial \alpha_{ww}}{\partial Q_i}\right)\right] \tag{4}$$

The expressions for (S_i) and (ρ_i) correspond, respectively, to plane-polarized, incident light in the direction perpendicular to the electric field and to its propagation direction.[36] However, the absolute differential Raman scattering cross section (in m^2/sr) corresponds to the measured absolute Raman intensity and is given by.[30,35]

$$\frac{\partial \sigma_i}{\partial \Omega_i} = \frac{(2\pi)^4}{45}(\nu_o - \nu_i)^4 \frac{h}{8\pi^2 c \nu_i B_i} S_i \tag{5}$$

Where, B_i represents the temperature factor which accounts for the intensity contribution of excited vibrational states and is represented by the Boltzmann distribution.

$$B_i = 1 - \exp\left(-\frac{h\nu_i c}{kT}\right) \tag{6}$$

In Eqns (5) and (6), h, k, c and T are Planck and Boltzmann constants, speed of light and temperature in Kelvin, respectively; ν_o is the frequency of the laser excitation line ($\nu_o = \frac{1}{\lambda}$), where λ_0, ν_i are wavelength of laser and the frequency of normal mode, respectively. The theoretical Raman intensity (infrared (IR)), which simulates the measured Raman spectrum, can be calculated according to the formula

$$I_i^R = C(v_o - v_i)^4 . v_i^{-1} . B_i^{-1} . S_i \quad (7)$$

Where, S_i is the Raman scattering activity of the normal mode Q_i calculated by DFT methods.[30] The presented theoretical Raman intensities have been computed assuming B_i equal 1. The theoretical Raman spectra have been calculated by phonon code implemented in.[30] The simulated spectra were plotted using a Lorentzian band shape with a half-width at half-height (FWHM) of 5 cm^{-1}.

Results and discussion

Structure of rutile SnO_2

In order to describe proper lattice dynamical behavior and its pressure dependence, we have first optimized (lattice constants and atomic internal co-ordinates) the rutile structure of SnO_2 at several pressures up to 20 GPa by minimizing the crystal total energy obtained for different volumes. The tetragonal symmetry has been enforced throughout the simulations. The calculated zero pressure structural parameters are in good agreement with previous experimental and theoretical results.[4,5,19,37] These lattice parameters (a and c) were used to fit an equation of states using Birch–Murnaghan third-order equation[39] which yield zero pressure bulk modulus B_0 and its first derivative B′. Table 1 summarizes the results for bulk modulus B_0, its first derivative B′ and lattice parameters a and c for rutile SnO_2 along with the available experimental[4,5] and other theoretical[19] results. There is a reasonably good agreement between the present and previous results.

Elastic instability in rutile SnO_2

In order to investigate the elastic instability in rutile SnO_2 (stishovite) responsible for the transition, we have optimized tetragonal unit cell at a given pressure by slightly distorting under an orthorhombic strain and reoptimizing the ionic positions in the strained lattice similar to the one used by Karki *et al.*[38] for rutile to $CaCl_2$ phase transition in silica. This methodology has also been used by Tsuchiya *et al.*[34] to investigate the phase boundaries of high-pressure polymorphs of silica. The calculated pressure variation of elastic constants of the rutile SnO_2 is plotted in Fig. 1 along with the experimentally derived elastic constants from Brillouin spectroscopy.[18] There is reasonably good agreement between present theory and experiment. Figure 2 shows the variation of shear of modulus, $(C_{11}–C_{12})/2$ which reveals that the shear modulus becomes negative at high pressure with $(C_{11}–C_{12})/2 = 0$ at 14.9 GPa, implying that this is transition pressure. This figure also

Table 1. Ground state structural parameters of rutile-type SnO_2

	a(Å)	c(Å)	x	B(GPa)	*B′*
Present cal.	4.7398	3.1871	0.3054	209.40	4.8
[a]Theoretical	4.6809	3.1790	0.3056		
[b]X-Rays	4.7367	3.1855	0.3070		
[c]Neutron	4.7374	3.1864	0.3056		

[a]Ref[19]
[b]Ref[4]
[c]Ref[5]

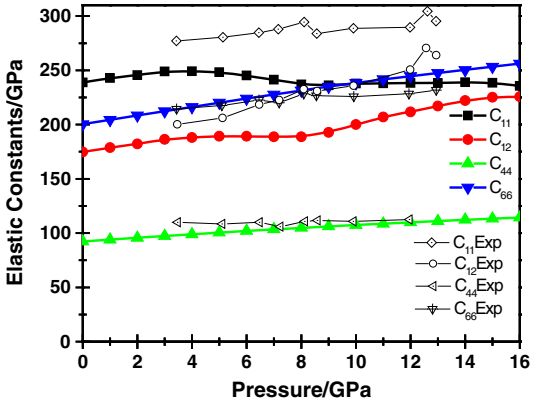

Figure 1. Calculated elastic constants together with the Brillouin spectroscopy data.[18]

indicates the experimentally obtained shear modulus from ref.[18] and shows a reasonably good agreement in terms of both values and trend. The transition pressure even obtained from the interpolation of Brillouin data (14.6 GPa) is in excellent agreement. This indicates a strongly coupling between Raman modes and elastic constants[38] as we did not found calculated shear modulus to become softer with pressure in the case of ions not allowed to relax in the distorted cell

Zone centre phonons of rutile SnO_2

The main part of the present calculations was to monitor the pressure dependence of the phonon frequencies, i.e. the stability of the crystal lattice with respect to small displacements and Raman intensity. The Landau theory of phase transition[40] establishes certain restrictions on the possible low symmetry group (high-pressure phase) with respect to the parent high symmetry rutile phase with space group $P4_2/mnm$. To understand the changes that occur in the phonon spectrum of rutile SnO_2 at high pressure, we have calculated the full PDC along with the total phonon density of states at several pressures up to 20 GPa using first principles calculations within density functional theoretical formulations. It is an established fact that the frequency of Raman active mode B_{1g} (the lowest optical branch) decreases with increasing pressure, contrary to the typical behavior observed for other Raman active phonon modes in the case of rutile

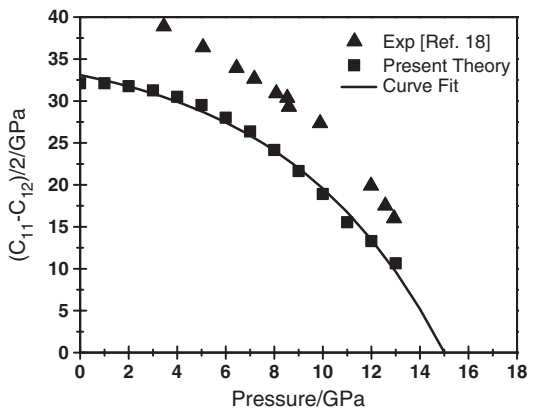

Figure 2. Pressure dependence of shear modulus $(C_{11}–C_{12})/2$ of the rutile structure SnO_2. The triangle represents the experimental values. Curve fit is the nonlinear curve fitting using the equation $= A_1 \exp\left(^{-x}/_{t_1}\right) + y_0$ n, where $A_1 = -3.8415$, $t_1 = -6.6310$, $y_0 = 36.9933$GPa.

dioxides.[18,36,41–44] This softening of the B_{1g} Raman mode indicates a structural instability, which is the precursor of phase transition.

To assess the behavior of all phonon modes at the zone centre, we analyze their pressure dependency. According to group theory, the rutile structure has the following phonon modes at centre of the BZ:

$$\Gamma = 2A_{2u}(IR) + 4E_u(IR) + B_{1g}(R) + 2B_{1u} + A_{2g} + E_g(R) + A_{1g}(R) + B_{2g}(R) \quad (8)$$

Where, R and IR correspond to Raman and infrared active modes. *A* and *B* modes are nondegenerate, while *E* modes are doubly degenerate. The g and u represent the symmetric and antisymmetric modes with respect to a centre of inversion. One A_{2u} and one E_u modes correspond to zero frequency acoustic modes, and rest are optical modes. The present calculated LDA and GGA frequency for all phonon modes for rutile SnO_2 at the Γ-point (zone centre) of the BZ are listed in Table 2 along with previous theoretical[19,29,46,47,49] and experimental Raman[37,47,49] data. Table 2 depicts an overall good agreement between present calculations using both LDA and GGA and previous data in the same group. The difference in the results obtained with LDA and GGA calculations is within the range of ~3–8% variations. Hence, we performed all detailed calculations with GGA, which are in over all better agreement with experimental results. This can also be justified from the fact that the GGA ensures better agreement with the experimental data than LDA in terms of energetices of low-pressure polymorphs of silica and is successful in predicting the phase diagram and PDC of three high-pressure polymorphs of SiO_2.[34]

Additionally, the evolution of phonon modes with pressure is presented in Fig. 3. The figure depicts that the frequencies of all phonon modes increase except the Raman active mode B_{1g} and transverse acoustic (TA) mode A_{2u} which soften with pressure. The results presented in this figure support the original hypothesis, where it is postulated that the instability of the rutile phase at high pressure could be related with the softening of B_{1g} Raman active mode and shear modulus, which describes the TA soft mode along [110] with B_{1g} symmetry. However, there is a difference in the transition pressures derived from crossing point in this figure for B_{1g} Raman active phonon and TA soft modes. The frequency of TA mode vanishes at ~10 GPa. The B_{1g} Raman active mode starts softening with pressure, and finally its frequency vanishes at ~12 GPa in contrast to the 7 GPa of Ref..[19] The phase transition in rutile SnO_2 is combined effect of both resulting from the coupling between Raman active mode B_{1g} and the TA mode (shear modulus). This means that the pressure of 10 GPa starts destabilizing the rutile SnO_2 lattice and complete transformation to the $CaCl_2$ phase at 12 GPa close to the experimental values[4,29,37] in contrast to the previous results. Hence, the second-order phase transition from rutile to $CaCl_2$-type structure is related with the ferroelastic phase transition[19] arising from the coupling between Raman active B_{1g} mode and shear modulus. The coupling between B_{1g} mode and the shear modulus results from the rigid unit mode picture of the SnO_6 octahedra normally having lower energy and becomes unstable under pressure.[38] In Fig. 3, we present the square of the frequency with pressure, which fits straight line and leads to the freezing of the phonon amplitude at the transition pressure and leading to high-pressure $CaCl_2$ phase.

Table 3 gives the calculated mode Grüneisen parameter of the phonon modes along with the other theoretical[19] and experimental data.[37] We find that the present values explain better to the

Table 2. Phonon mode frequencies in Thz at the zone centre point of rutile SnO_2 along with previous experimental and calculated data

	Present calculations		Experimental		Theoretical				
Mode	LDA	GGA	Exp[a]	Expt[b]	Cal[a]	Cal[c]	Cal[d]	Cal[e]	Cal[f]
A_{1g}	19.36	20.01	19.13	19.10	19.37	18.84	20.30	19.17	19.13
A_{2g}	8.94	13.86	-	-	11.95	14.64	-	-	10.98
B_{1g}	4.320	3.00	-	3.63	3.00	3.68	5.52	3.80	3.14
B_{2g}	22.23	22.38	23.45	23.41	22.54	23.03	23.35	22.81	22.84
E_g	14.59	14.58	14.08	14.27	13.22	14.93	14.27	13.53	14.08
$B_{1u}^{(1)}$	3.93	6.51	-	-	4.20	4.48	-	-	4.40
$B_{1u}^{(2)}$	17.47	17.86	-	-	15.14	18.09	-	-	17.54
$A_{2u}(TO)$	14.23	13.89	14.30	-	15.35	14.30	14.00	15.39	13.82
$E_u^{(1)}(TO)$	5.34	6.51	7.32	-	7.08	6.98	7.08	7.43	7.24
$E_u^{(2)}(TO)$	8.16	8.31	8.78	-	8.90	9.14	9.32	10.14	8.57
$E_u^{(3)}(TO)$	18.24	18.60	18.53	-	19.52	19.41	16.82	19.82	18.43
$A_{2u}(LO)$	14.22	13.89	21.13	-	20.60	21.09	21.29	19.63	19.70
$E_u^{(1)}(LO)$	8.16	8.31	8.27	-	8.03	7.40	8.69	7.43	8.36
$E_u^{(2)}(LO)$	8.16	10.18	10.97	-	11.30	14.32	12.11	12.77	12.18
$E_u^{(3)}(LO)$	18.24	20.01	23.08	-	22.48	22.12	21.20	19.82	21.09

[a]Ref[49]
[b]Ref[37]
[c]Ref[29]
[d]Ref[46]
[e]Ref[47]
[f]Ref[19]

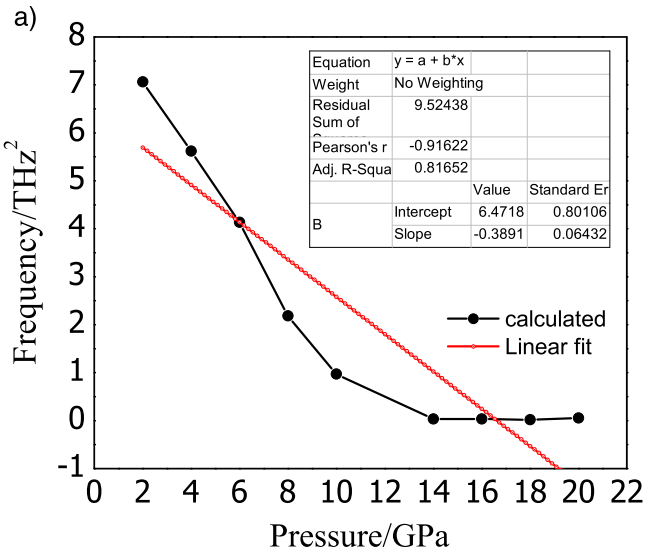

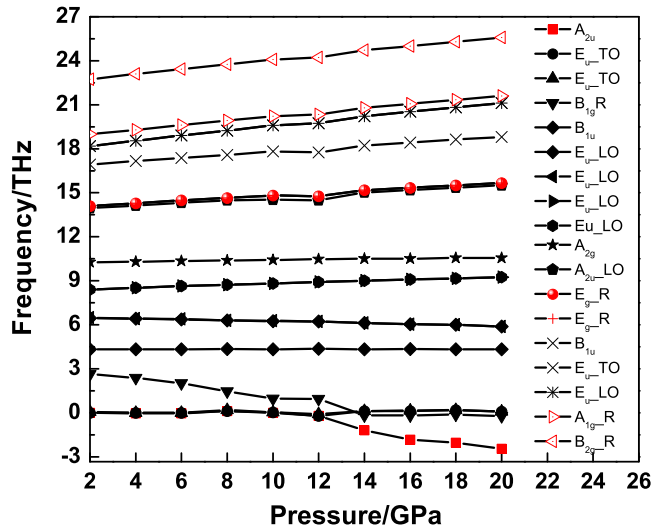

Figure 3. Pressure variation of zone centre modes for rutile SnO_2, (a): Pressure variation of B_{1g} mode for rutile SnO_2.

Table 3. Grüneisen parameters ν_i of the phonon modes of rutile SnO_2

Mode	Present calculation	Theory[a]	Exp[b]
A_{1g}	1.617	1.33	3.64
A_{2g}	0.354	0.63	-
B_{1g}	−10.82	−14.17	−10.44
B_{2g}	1.463	1.49	2.58
E_g	1.300	1.29	3.20
$B_{1u}^{(1)}$	0.0098	0.26	-
$B_{1u}^{(2)}$	1.3098	1.56	-
$A_{2u}(TO)$	1.330	1.32	-
$E_u^{(1)}(TO)$	−1.0067	−0.62	-
$E_u^{(2)}(TO)$	1.1463	1.14	-
$E_u^{(3)})(TO)$	1.901	1.91	-

[a]Ref[19]
[b]Ref[37]

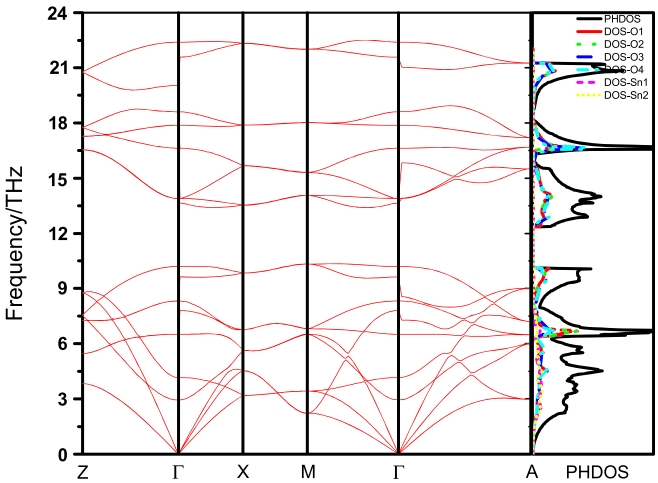

Figure 4. Phonon dispersion curves and phonon density of states of SnO_2 in rutile phase at ambient pressure.

experimental data particularly for the responsible B_{1g} mode for phase transition. For other modes, the present and previous theoretical calculations agree well.

PDC and dynamical stability of rutile SnO_2

In order to make a further check on the stability of the rutile SnO_2 phase, we have calculated phonon frequencies for various symmetry directions in the BZ, i.e. PDC at the pressure close to the transition pressure. We found that all phonon frequencies are real at the pressures of few GPa below the transition pressure (Figs. 4 and 5). The right panel of these curves presents corresponding phonon density of states. However, we observe that the frequency of the B_{1g} Raman active (the lowest optical branch) mode of rutile SnO_2 at zone centre decreases with increasing pressure and becomes fully imaginary at the pressure 12 GPa (Fig. 6). This mode accounts for the libration of columns of edge-sharing SnO_6 octahedra in rutile SnO_2 similar to the one

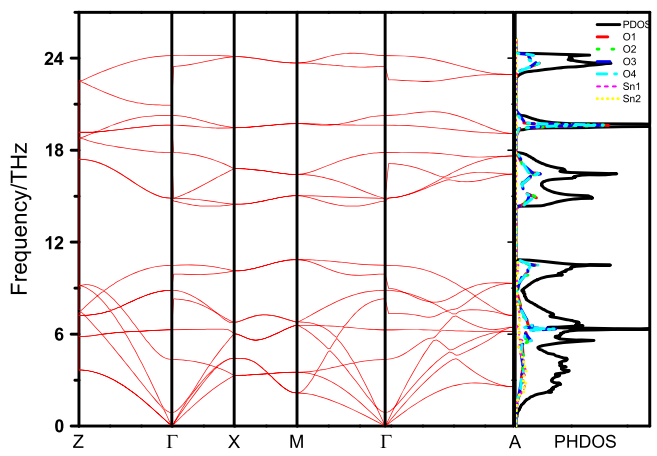

Figure 5. Phonon dispersion curves and phonon density of states of SnO_2 in rutile phase at 10 GPa pressure.

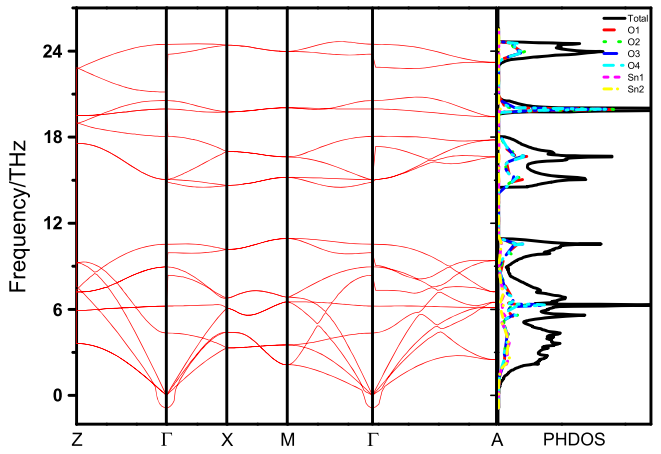

Figure 6. Phonon dispersion curves and phonon density of states of SnO_2 in rutile phase at transition pressure (12GPa).

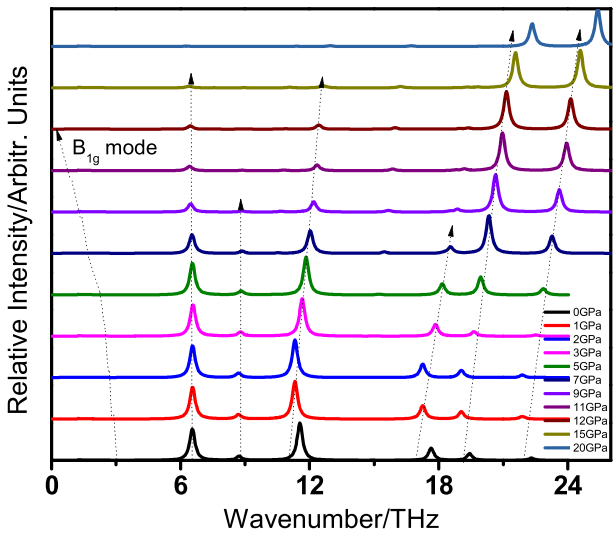

Figure 7. Calculated high-pressure onset Raman spectra up to 20 GPa for rutile SnO_2. This figure is available in colour online at wileyonlinelibrary.com/journal/jrs

observed in the case of SiO_6 octahedra in the rutile SiO_2.[34,38] A close look of the PDC in Fig. 6 depicts that the TA phonon branch (elastic mode) which corresponds to the shear modulus[34,38] is imaginary in the vicinity of zone centre arising from the interaction of Raman active B_{1g} mode mainly responsible for destabilizing the tetragonal rutile SnO_2. This phase transition pressure of 12 GPa is in good agreement with experiment in contrast to previous reported transition pressure obtained from the similar method.[19]

The PDC presented at zero pressure is in overall good agreement with earlier calculated PDC[19] and available experimental data.[49] There are however minor differences, with previous calculations such as the lack of crossing of $Eu^{(1)}$ mode in Γ-X direction and almost degenerate low-lying acoustic modes in X-M direction of the BZ. The phonon density of states reflects all general features of PDC. The *Sn* and *O* atoms vibrations almost equally contribute to the phonon density of states up to 10.5 THz, while the major contribution to 12–23 THz is due to *O* atom vibrations.

In order to clarify the structural mechanism of the phase transition and to obtain more insights in to the stability of the phase at higher pressures, we have calculated the theoretical Raman and IR spectra (intensity *vs* frequency curve) up to 20 GPa for rutile SnO_2. Figure 7 presents the Raman spectra between ambient and 20 GPa calculated using the methodology discussed in section II. All characteristic peaks of the rutile are seen in the ambient pressure spectra. Our calculations properly reproduce which Raman mode has the largest intensity, which one the second largest and so on. The intensity of the B_{1g} Raman mode is very poor as this band has intensity less than 0.001 of the A_{1g} mode.[49] Therefore, we plot only the intensity of B_{1g} mode with pressure in Fig. 8. Figure 8 depicts that the intensity of B_{1g} mode decreases with pressure and finally vanishes close to phase transition. Further, as seen in inset of Fig. 8, the representation of the eigen vector B_{1g} in the structure along *z*- axis clearly brings out that the *O* anions rotate perpendicular to the [001] direction, where *Sn* atoms remain fixed, resulting in an orthorhombic distortion of the tetragonal unit cell similar to the one recently observed in rutile FeF_2.[50]

At high pressures, the B_{1g} mode not only diminishes close to the phase transition pressure around 12 GPa but also shifts to lower wave numbers. However, the frequency of other modes increases as per the normal expectation due to compressed bands under the influence of pressure. For the current research, a more important feature is the pressure dependence of the Raman line intensities calculated from the component of Raman tensor. We find while intensity of several peaks increases, the peak intensity for several peak diminishes at around the phase transition pressure of 12 GPa. These are indicative features of phase transition. To have a clear evolution of peaks and its intensity with pressure, we analyze a three-dimensional pressure-dependent Raman intensity plots (not shown here). This clearly brings out the relative intensity of peaks. We also present the pressure-dependent IR intensity plot of rutile SnO_2 in Fig. 9. This figure does not however show any disappearance of modes, and its intensity which is quite obvious but shows the pressure-dependent shift of peak positions.

Finally, the better prediction of high-pressure behavior and transition pressure of rutile SnO_2 can be attributed mainly to three features: (1) The use of exchange correlational functional; while we used GGA exchange correlational functional in present calculation, the earlier calculation was done using LDA functional.[19] It is an established fact that the LDA gives smaller lattice constants than GGA and experiment at given pressure, which results into the lower transition pressure than GGA and

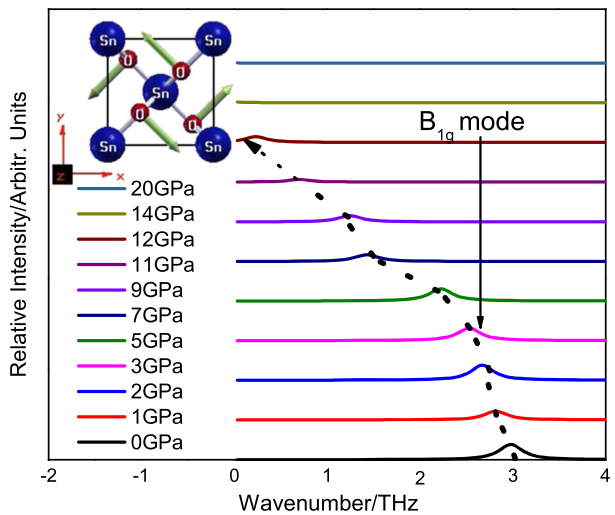

Figure 8. Calculated high-pressure Raman active B_{1g} mode up to 20 GPa for rutile SnO_2. This figure is available in colour online at wileyonlinelibrary.com/journal/jrs

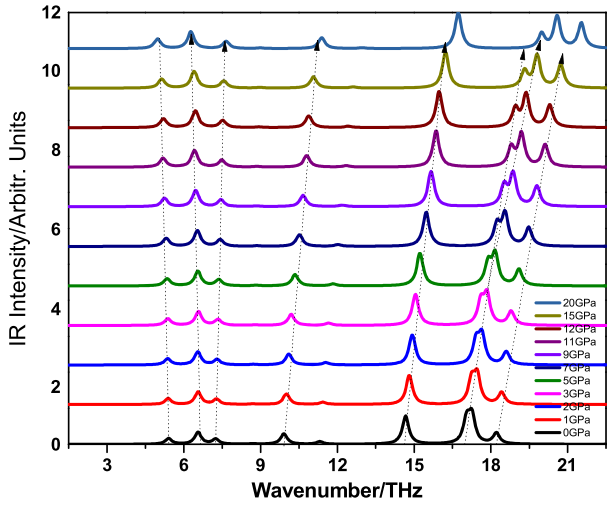

Figure 9. Calculated high-pressure onset Infrared spectra up to 20 GPa for rutile SnO_2. This figure is available in colour online at wileyonlinelibrary.com/journal/jrs

experiment. (2) The phonon calculations are done using DFPT based on linear response theory in contrast to the previous study which used frozen phonon or direct method. The linear response theory which provides an efficient approach for calculating the vibrational properties uses the same unit cell which is used for ground state calculations. Since the use of supercells is eliminated, points with little or no symmetry in the BZ can be handled. However, in the case of frozen phonon method, only the phonon wave vectors that lie along high symmetry directions and that correspond to reasonably sized supercells can be considered, and hence it becomes difficult to determine accurately the quantities such as phonons, electron–phonon coupling parameters, real space force constants etc. as it involve integration over the wave vector throughout the BZ[51,52] (3) As the rutile to $CaCl_2$ transition involves the softening of the $(C_{11}–C_{12})/2$ shear modulus and Raman active B_{1g} mode with pressure, the optimization of all structural parameters including the shape of the cell (i.e. the lattice constants and free ionic positions) is essential as [38] implemented in the present theory.

Summary

In summary, we have presented a systematic lattice dynamical study of the pressure-induced phase transition in rutile SnO_2 using first principles DFPT based on plane wave pseudopotential technique. We have studied the PDC, zone centre phonons and Raman and IR intensities up to pressure 20 GPa. The ferroelastic transition from the rutile to $CaCl_2$-type structure was confirmed. The soft mode behavior of B_{1g} mode in the rutile structure was observed at transition pressure. We found that the results of the present calculations on PDC and the transition pressure is reproduced and compare very well with the available experimental data in contrast to previous calculations. The rutile to $CaCl_2$ transition involves the softening of shear modulus and Raman active B_{1g} mode with pressure therefore the optimization of structure (lattice constants and atomic coordinates) under symmetry constrains at different pressure is essential for a detailed understating of transition. The Raman and IR intensities plots with pressure show shift in the peaks positions towards the higher frequency side except the Raman active B_{1g} mode which not only shift towards low wavenumber but the intensity also diminishes. Furthermore, our results show that the calculation of the lattice dynamics can be a reliable way to predict transition pressure by monitoring the pressure dependence of phonon frequencies. Finally, the high-pressure study or accurate prediction of phase transition in SnO_2 may help in understanding the phase transitions of SiO_2 as this could be involved in some of the seismic anomalies observed in the lower mantle of the earth. Further, our present theoretical calculations reproduce the experimentally determined pressure response of the vibrational modes of rutile SnO_2 and hence give confidence for the accurate predictive power of first principles calculations.

Acknowledgements

The financial support from the DST-RFBR and DAE-BRNS is highly appreciated for this work. PKJ is thankful to UGC, New Delhi for UGC Research award and also grateful to the TWAS, CAS-ITP, China for the hospitality and financial support during which part of the work was completed.

References

[1] J. Robertson, *J. Phys. C: Solid State Phys.* **1979**, *12*, 4767.
[2] Ph. Barbarat, S. F. Matar, G. Leblevennec, *J. Mater. Chem.* **1997**, *7*, 2547.
[3] Ph. Barbarat, S. F. Matar, *Comput. Mater. Sci.* **1998**, *10*, 368.
[4] J. Haines, J. M. Legar, *Phys. Rev. B.* **1997**, *55*, 11444.
[5] A. A. Rolzan, C. Fong, B. J. Kennedy, C. J. Howard, *Acta. Cryst. B.* **1997**, *58*, 373.
[6] L. Nagel, M. O'Keeffe, *Mater. Res. Bull* **1971**, *6*, 1317.
[7] Y. Tsuchida, T. Yagi, *Nature* **1989**, *340*, 217.
[8] K. J. Kingma, R. E. Cohen, R. J. Hemley, H. K. Mao, *Nature* **1995**, *374*, 243.
[9] J. Haines, J. M. Léger, C. Chateau, R. Bini, L. Ulivi, *Phys. Rev. B.* **1998**, *58*, R2909.
[10] D. Andrault, G. Fiquet, F. Guyot, M. Hanfland, *Science* **1998**, *282*, 720.
[11] R. J. Hemley, J. Shu, M. A. Carpenter, J. Hu, H. K. Mao, K. J. Kingma, *Solid State Commun.* **2000**, *114*, 527.
[12] J. Haines, J. M. Léger, C. Chateau, A. S. Pereira, *Phys. Chem. Miner.* **2000**, *27*, 575.
[13] J. Haines, J. M. Leger, O. Schulte, *J. Phys. Condens. Matter* **1996**, *8*, 1631.
[14] J. Haines, J. M. Leger, *Phys. Rev. B* **1997**, *55*, 11144.
[15] S. Ono, E. Ito, T. Katsura, A. Yoneda, M. J. Walter, S. Urakawa, W. Utsumi, K. Funakoshi, *Phys. Chem. Miner.* **2000**, *27*, 618.
[16] S. Ono, K. Funakoshi, A. Nozawa, T. Kikegawa, *J. Appl. Phys.* **2005**, *97*, 073523.
[17] S. R. Shieh, A. Kubo, T. S. Duffy, V. B. Prakapenka, G. Shen, *Phys. Rev. B* **2006**, *73*, 014105.
[18] H. Hellwig, A. F. Goncharov, E. Gregoryanz, H.-k. Mao, R. J. Hemley, *Phys. Rev. B* **2003**, *67*, 174110.
[19] K. Parlinski, Y. Kawazoe, *Eur. Phys. J. B* **2000**, *13*, 679.
[20] R. Saniz, H. Dixit, D. Lamoen, B. Partoens, *Appl. Phys. Lett.* **2010**, *97*, 261901.
[21] S. F. Matar, D. Jung, M. A. Subramanian, *Solid State Com.* **2012**, *152*, 349.
[22] K. Suito, N. Kawai, Y. Masuda, *Mater. Res. Bull* **1975**, *10*, 677.
[23] S. Endo, S. Nitawaki, T. Shige, Y. Akahama, T. Kikegawa, O. Shimomura, *High Press. Res.* **1990**, *4*, 408.
[24] R. E. Peirls, Quantum Theory of Solids, Clarendon, Oxford, **1956**.
[25] M. Born, K. Huang, The Dynamical Theory of Crystal Lattices, Clarendon, Oxford, **1954**, pp. 153.
[26] P. W. Anderson, in Fizika Dielektrikov (Ed.: G. N. Skanavi) Acad. Nauk SSSR, Moscow, **1960**; W. Cochran, *Adv. Phys.* **1960**, *9*, 387.
[27] S. Ono, K. Mibe, *Phys. Rev. B.* **2011**, *84*, 054114.
[28] J. Petzelt, V. Dvorak, *J. Phys. C: Solid State Phys.* **1976**, *9*, 1571.
[29] M. E. Striefer, G. R. Barsch, *Phys. Stat. Sol. B* **1975**, *67*, 143.
[30] P. Giannozzi *et al.*, QUANTUM ESPRESSO: a modular and open-source software project for quantum simulations of materials, *J. Phys. Condens. Matter* **2009**, *21*, 395502; see http://www.quantum-espresso.org
[31] J. P. Perdew, K. Burke, M. Ernzerhof, *Phys. Rev. Lett.* **1996**, *77*, 3865.

[32] D. Vanderbilt, *Phys. Rev. B* **1990**, *41*, 7892.
[33] S. Baroni, S. de Gironcoli, A. dal Corso, P. Giannozzi, *Rev. Mod. Phys.* **2001**, *73*, 515.
[34] T. Tsuchiya, R. Caracas, J. Tsuchiya, *Geophysical Res. Lett.* **2004**, *31*, L11610.
[35] G. Placzek, in Handbuch der Radiologie, edited by E. Marx (Akademische Verlagsgesellschaft, Leipzig, **1934**), pp. 205 English Translation by Ann Werbin, UCRL Trans-526(L).
[36] P. L. Polavarapu, *J. Phys. Chem.* **1990**, *94*, 8106.
[37] J. P. Peercy, B. Morosin, *Phys. Rev.* **1973**, *7*, 2779.
[38] B. B. Karki *et al*., *Phys. Rev. B* **1997**, *55*, 3465.
[39] F. Birch, *J. Geophys. Res. B.* **1978**, *83*, 1257.
[40] L. D. Landau, E. M. Lifshitz, Statistical Physics, Pergamon, New York, **1961**.
[41] H. Wang, X. Liu, Y. Li, Y. Liu, Y. Ma, *Solid State Comm.* **2011**, *151*, 1475.
[42] S. S. Rosenblum, W. H. Weber, B. L. Chamberland, *Phys. Rev. B* **1997**, *56*, 529.
[43] B. R. Maddox, C. S. Yoo, D. Kasinathan, W. E. Pickett, R. T. Scalettar, *Phys. Rev. B* **2006**, *73*, 144111.
[44] A. Togo, F. Oba, I. Tanaka, *Phys. Rev. B* **2008**, *78*, 134106.
[45] P. D. Borges, L. M. R. Scolfaro, H. W.. Leite Alves, E. F.. da Silva Jr, *Theor Chem Acc* **2010**, *126*, 39.
[46] F. Gervais, W. Kress, *Phys. Rev. B* **1985**, *31*, 4809.
[47] T. Sato, T. Asari, *J. Phys. Soc. Jpn.* **1995**, *64*, 1193.
[48] Lee C., X. Gonze, *J. Phys. Condens. Matter* **1995**, *7*, 3693.
[49] R. S. Katiyar, P. Dawson, M. M. Hargreave, G. R. Wilkinson, *J. Phys. C. Solid. St. Phys.* **1971**, *4*, 2421.
[50] S. López-Moreno, A. H. Romero, J. Mejía-López, A. Muñoz, I. V. Roshchin, *Phys. Rev. B* **2012**, *85*, 134110.
[51] S. Y. Savrasov, *Phys. Rev. B* **1996**, *4*, 16470
[52] K. Kunc, I. Loa, K. Syssen. R. K. Kremer, K. Ahn, *J. Phys. Condens. Matter* **2001**, *13*, 9945.